Journal of
Applied
Crystallography
ISSN 0021-8898

Received 17 December 2003
Accepted 12 November 2004

Ostwald ripening of cobalt precipitates in silica aerogels? An ultra-small-angle X-ray scattering study

Artur Braun,[a]*‡¶ Jan Ilavsky,[b] Brian C. Dunn,[c]¶ Pete R. Jemian,[d] Frank E. Huggins,[a]¶ Edward M. Eyring[c]¶ and Gerald P. Huffman[a]¶

[a]Department of Chemical and Materials Engineering, University of Kentucky, Lexington KY 40506, USA, [b]Department of Chemical Engineering, Purdue University, West Lafayette, IN 47907, USA, [c]Department of Chemistry, University of Utah, Salt Lake City, UT 84112, USA, and [d]Frederick Seitz Materials Research Laboratory, University of illinois at Urbana-Champaign, Urbana, IL 61801, USA. Correspondence e-mail: artur.braun@alumni.ethz.ch

Monolithic silica aerogels with radial symmetry were synthesized by supercritical drying, doped to 2% and 10% with cobalt, and reduced with hydrogen. All samples were investigated with ultra-small-angle X-ray scattering. The non-doped aerogels have three populations of scatterers with radii of gyration of about 10, 40 and 60–70 Å. The doped aerogels show an additional structure with a radius of gyration ranging from 1050 to 3000 Å. This structure causes intensity oscillations, thus revealing a relatively narrow size distribution. Scattering curves of the 10%-doped aerogels fitted well to a Lifshitz–Slyozov–Wagner particle size distribution, thus revealing that Ostwald ripening might have occurred during aerogel preparation. The same range also shows differences depending on whether the samples were reduced, or in their as-prepared condition. Scattering curves obtained from the cylinder-axis region were different from the scattering curves obtained from the sample boundary, indicating a process-dependent skin effect.

1. Introduction

Small-angle X-ray scattering (SAXS) has been used for many years to characterize highly dispersed, supported catalysts (Bazin *et al.*, 2000; Lorenz *et al.*, 1998; Haubold *et al.*, 1996, 1999; Schlenter, 1996; Benedetti *et al.*, 1999). Catalyst supports are typically highly porous materials, such as active C atoms, high-surface-area silica or aluminium oxides, zeolites, and carbon or silica aerogels. While high-surface-area materials theoretically allow for high dispersion with sufficient active catalyst sites, it remains an open question whether these sites are actually accessible to fluids that have to react catalytically.

The presence of sufficient diffusion channels of adequate size and connectivity is a critical requirement for catalysts in order to maintain mass transport of reactants and reaction products during catalyst activity, and this is at the cost of the number of active sites. Connected empty pore space for mass transport and high surface area for catalyst support are thus reciprocally related quantities that have to be optimized from case to case, depending on the catalyst support. In fact, the search for optimized catalysts and catalyst supports is still today an ongoing quest. Aerogels are expected to have larger pores than the other materials mentioned before. In particular, they contain a significant amount of so-called mesopores, pores with sizes ranging from 20 to 500 Å (IUPAC, 1985), small enough to provide a high surface area, but still so big that diffusion resistances do not become as critical as with micropores.

Aerogels have been studied with small-angle scattering for several decades (Schaefer & Keefer, 1986; Vacher *et al.*, 1988; Emmerling & Fricke, 1992; Marliére *et al.*, 2001). SAXS is the diffuse and elastic scattering of monoenergetic X-rays under an angle typically lower than half the angle of the lowest indexed non-specular Bragg reflection. It serves to resolve inhomogeneities such as particles and pores in a matrix on a length scale from nanometres to micrometres. The resolution of structures larger than, say, 500 Å, requires additional experimental effort. This technique is then called USAXS and permits the resolution of structures with sizes in the micrometre range.

The present study deals with the ultra-small-angle X-ray scattering (USAXS) characterization of a silica-based aerogel, which serves as a support for cobalt catalysts. It was prepared as a potential candidate for cobalt-based Fischer–Tropsch catalysts for the production of low-sulfur synthetic diesel from syngas (a mixture of hydrogen and carbon monoxide).

We have studied the non-doped and Co-doped aerogels with USAXS and found characteristic structural features, such

‡ Correspondence address: Suite 107 Sam J. Whalen Bldg, 533 South Limestone Street, Lexington KY 40506, USA.
¶ Member of the Consortium for Fossil Fuel Science, Lexington, KY 40506, USA.

as micropores of about 15 Å, and mesopores of about 50 Å size. The deposition of nanosized catalyst particles is clearly confirmed. Most noteworthy, Co precipitations of 1000 and 1700 Å size were found in the doped aerogels. We also found that the Co-doped aerogel from the sample center differs from material that is found at the outer boundary, in line with the visual and apparent radial color gradient of the doped aerogels.

Coagulation and coarsening of metal clusters in aerogels by Ostwald ripening was recently reported (Martino *et al.*, 1999). Particle sizes in systems governed by Ostwald ripening follow a characteristic distribution, which can be analytically derived from first principles [Lifshitz–Slyozov–Wagner (LSW) distribution (Lifshitz & Slyozov, 1961; Wagner, 1961)]. We observe that this distribution fits our data very well, and hence believe that Ostwald ripening might also occur in our system.

The analysis of the data will be presented in two parts. The first part describes general features of the scattering curves, derived from 'manual' analysis, *i.e.* subtraction of Porod scattering and Guinier analysis. The second part presents quantitative analysis, based on beamline-specific software macros with unified fits (Beaucage, 1995) for power laws and Guinier ranges, and fits with particle size distributions.

2. Experimental

2.1. Aerogel sample preparation

Undoped and Co-doped silica aerogels were prepared by modifications of published procedures (Russo & Hunt, 1986; Casula *et al.*, 2003). Briefly, a sol of tetramethoxysilane (TMOS, Aldrich, 98%) in methanol (Aldrich, spectrophotometric grade) was prepared by combining 15 ml each of TMOS and methanol. A solution of water (Aldrich, BPLC grade), methanol, and NH_4OH (Mallinckrodt, reagent grade) was prepared by combining 7.5 ml of methanol, 6 ml of water, and 0.750 ml of 2.8% NH_4OH. The two solutions were combined with vigorous stirring, transferred into cylindrical polyethylene forms, and allowed to gel. The molar ratio of the final mixture was 3:9:1 for water:methanol:TMOS and the gelation time was approximately 5 min. The gels were aged in their sealed forms for three days. For undoped gels, the gels were removed from their forms and solvent exchanged with absolute ethanol (Aaper) three times for at least 3 h each time. The ethanol was exchanged for acetone (Mallinckrodt, AR grade) three times for at least 3 h each time. The acetone-filled gel was placed in an acetone-filled 500 ml autoclave and the acetone was replaced with liquid CO_2 (Airgas, SFC grade) by flowing CO_2 through the autoclave for 6 h or until no further acetone was detected in the effluent. The autoclave was heated to 333 K to transform the CO_2 into a supercritical fluid (T_c = 241.9 K, p_c = 72.8 atm; 1 atm = 101.325 kPa) and the pressure inside the autoclave was maintained at 102 atm with a back-pressure regulator. While maintaining the temperature above the critical temperature, the pressure inside the autoclave was released over 4 h. The autoclave was cooled to room temperature and the aerogel removed. The volume of the aerogel was approximately 90% of the original gel and remained monolithic through the entire process. For Co-doped aerogels, the wet gels were solvent exchanged with absolute ethanol three times for at least 3 h each time. The gels were then loaded with $Co(NO_3)_2$ (Fischer, reagent grade) by exchanging the absolute ethanol with a solution of $Co(NO_3)_2$ dissolved in ethanol. The concentration and volume of the cobalt-containing ethanol solution was chosen such that the cobalt concentration in the final aerogel would be 2% or 10%, respectively. After a single solvent exchange, the gels were loaded into a 50 ml autoclave filled with ethanol, purged with N_2, and pressurized to 13 atm with N_2. The autoclave was heated in a fluidized sand bath to 523 K at 5 K min^{-1}, then to 573 K at 1 K min^{-1}. The pressure inside the autoclave was allowed to increase to 136 atm and maintained at this pressure by means of a controlled leak.

Under these conditions of temperature and pressure, ethanol exists as a supercritical fluid (T_c = 516.1 K, p_c = 63.0 atm). When no further increase in pressure was observed, the autoclave had reached 573 K and the temperature was maintained for 1 h. While keeping the autoclave at 573 K, the pressure was slowly released over 2 h, then the autoclave was removed from the sand bath and allowed to cool in static air until room temperature was achieved. The aerogels produced in this manner showed the same reduction in volume as the CO_2-dried gels, were monolithic, and showed an unusual radial color variation. The color is caused by oxides of cobalt that result when $Co(NO_3)_2$ is heated above its decomposition temperature. Both the undoped and Co-doped aerogels were calcined in static air at 737 K for 12 h and the Co-doped aerogels were then reduced in a flowing stream of hydrogen at 737 K for 4 h.

2.2. USAXS

Ultra-small angle X-ray scattering (USAXS) was carried out at synchrotron radiation beamline 33-ID at UNICAT, Advanced Photon Source, Argonne National Laboratory. At this beamline, a Bonse–Hart setup allows one to record USAXS scattering curves using a photodiode detector with an angular resolution of 0.0001 $Å^{-1}$ in a q range from 0.0002 to 1.0 $Å^{-1}$. The upper resolution range is 5000 Å. The scattering vector q is a typically used quantity in small-angle scattering and relates to the diffraction angle (2θ), as known from X-ray diffraction, *via* the relation $q = (4\pi/\lambda)\sin\theta$, with X-ray wavelength λ. The data acquisition time for a scattering curve with 150 data points was typically 15 min per sample. Data points were distributed across the q range at distances determined by an algorithm described by Jemian & Long (1990). Scattering curves were recorded at X-ray energies of 7695 and 7710 eV. All USAXS data were fully corrected for all instrumental effects, including subtraction of blank sample background and photodiode dark current, constant flat background due to incoherent scattering, and desmearing. The supplied samples had cylinder-like shape and were cut in cylinder fragments with thicknesses of approximately 1 cm. Accurate sample thickness data are not known; scattered intensities are thus

given in arbitrary units. For skin studies, either the cylinder center (= no skin) or the cylinder boundary (= skin) was positioned in the X-ray beam, with the cylinder axis parallel to the X-ray beam. For all other cases, the cylinder axis of the sample was perpendicular to the beam, and the sample thickness at this position was at maximum.

3. Results and discussion

3.1. Non-doped aerogels

The scattering curve of the CO_2-dried aerogel is shown in Fig. 1 in a typical log–log plot. The q range extends from 0.0002 Å^{-1} to almost 1 Å^{-1}. Theoretically, structures are resolved on a length scale between 5 and 15000 Å, according to the relation $L = \pi/q$. The experimental resolution limit is here about 10000 Å. L is the length of an object in real space and q is the scattering vector. The overall structure of the scattering curve displays a steep power law at the far left and far right side of the scattering curve, *i.e.* very small and very large q values, with a plateau of intensity in the middle range.

We are interested in q regions where the intensity changes drastically. This is the central part of the bending region on the right side of the plateau, at about q = 0.02 Å^{-1}. A Guinier function (Guinier, 1939; Glatter & Kratky, 1982)

$$I(q) = NV^2 \Delta n_f^2 \exp(-q^2 R_g^2/3) \qquad (1)$$

was fitted to this region and yields a radius of gyration R_g of about 50 Å. This structure, caused by mesopores (IUPAC, 1985) with roughly the same R_g, was found for all aerogels investigated in this study. N is the number of pores in the irradiated sample volume, detected in this q range, V the volume of a single pore, and Δn_f^2 the X-ray scattering contrast between the pores and the silica matrix. R_g is the radius of gyration of the objects (pores or particles), which is the mean square distance from the center of electron density of a particle (in analogy to the momentum of inertia in mechanics):

$$R_g^2 = \int_V \rho(r_i) r_i^2 \, dV \Big/ \int_V \rho(r_i) \, dV. \qquad (2)$$

The radius of gyration is analogous to the radius of inertia in mechanics and describes the center of the electron distribution in the irradiated sample. For a sphere, R_g translates into the sphere radius as $R = (5/3)^{1/2} R_g$. From the characteristics of the scattering curve, it is not obvious what shape the objects in the scattering curve structure mentioned may have. However, if they were spheres, the radius would be 74 ± 10 Å.

The power law for the intensity variation for large q does not obey Porod's law (Porod, 1951, 1952*a*,*b*), *i.e.* q^{-4}. Instead, it shows a decay of $q^{-3.6}$, indicative of a rough internal surface of the aerogel on this length scale. Very close inspection of the scattering curve for q values larger than 0.1 Å^{-1} reveals minute deviations even from a power law. Thus, we have subtracted a constant scattering background as well as the observed power law function from the original scattering curve, in order to visualize better the scattering of objects in the aerogel [most likely the micropores (IUPAC, 1985)] on this length scale. The result of these subtractions is shown in Fig. 1, as a solid line at the very right end of the plot at $0.1 \leq q \leq 0.7$ Å^{-1}. It shows two humps with a relatively sharp intensity minimum between them; this could be indicative of a relatively sharp size distribution of spheres. Guinier analysis showed that spheres with a radius of 14 Å would model this structure very well. Fig. 2 shows the scattered intensity of this structure *versus* the product of q and the proposed sphere radius of 14 Å. For comparison, the structure factor of spheres, $S(q, R)$ (Rayleigh, 1911) with R = 14 Å, is also plotted:

$$S(q, R) = \{3[\sin(qR) - qr\cos(qR)]/(qR)^3\}^2. \qquad (3)$$

This structure function shows distinct intensity minima at $(2n + 1)$ multiples of $\pi/2$. Such minima become more pronounced as the underlying size distribution sharpens. In the present case, however, we believe that a relatively sharp size distribution of sphere-like pores of about 14 Å radius is observed. The EtOH-dried sample shows the same feature after back-

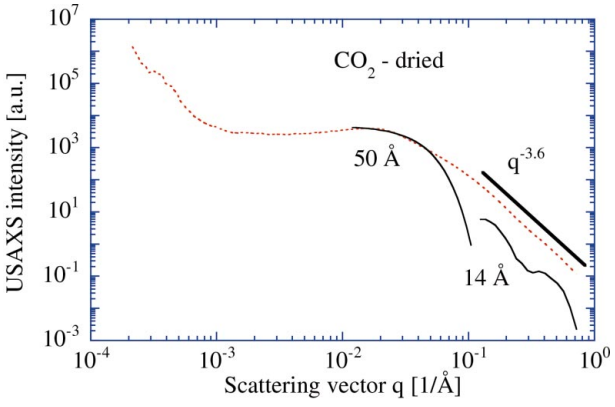

Figure 1
Log–log plot of CO_2-dried aerogel. Two least-squares fits of the Guinier function are marked with solid lines. The straight solid line to the right side is a power law function with −3.6 as the exponent of decay. The solid line below shows additional structures after subtraction of background scattering and the power law function. Numbers denote radii of gyration R_g.

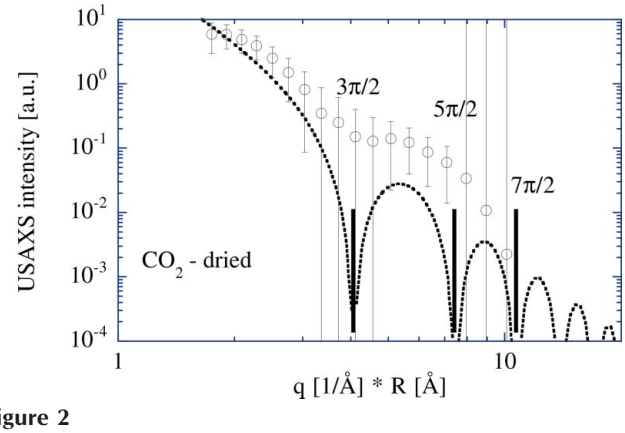

Figure 2
Comparison of micropore scattering of aerogel and the structure function of spheres with 14 Å radii. Vertical lines denote the expected positions of the intensity minima after equation (3). The ordinate axis is given in dimensionless units, with R = 14 Å.

ground and power law subtraction, with a sphere radius also of about 14 Å.

3.2. Doped aerogels

A comparison of the scattering curves of non-doped aerogel, and of aerogels doped with 2% and 10% cobalt is presented in Fig. 3. The most striking difference between the scattering curves of doped and non-doped samples is the presence of an additional structure in the q range of $0.001 \leq q \leq 0.006$ Å^{-1}. In this range, both doped samples show pronounced intensity humps with R_g of 1750 and 1040 Å for the 2%- and 10%-doped aerogels, respectively. For the latter case, the decay of intensity is more rapid. Also, intensity minima are observed in this range, indicative of a relatively sharp size distribution. The sample doped with 2% cobalt shows a broader hump and less pronounced intensity minima. We believe that this additional structure is incurred by clusters formed by the dopants, dendrite-like particles, with sizes of 2300 and 1350 Å, respectively.

The doped aerogels differed from the non-doped aerogels also in terms of their color and outer appearance. The non-doped aerogels had the typical bluish, opaque and diaphanous appearance, while the doped samples were brownish or greenish in color and appeared more robust, by virtue of their increased opacity.

We have already identified the micropores in the aerogel, as shown by the background- and power-law-subtracted scattering curve of the non-doped samples. These might act as hosts for the deposition of cobalt-rich clusters. On the other hand, precipitation and coagulation processes might occur, which form larger clusters, such as those found at about 1350–2300 Å in the doped aerogels.

Inspection of the large q tails of the scattering curves of the doped samples reveals, however, that they have a deviation of the scattered intensity from their initial power law (for $q \geq 0.4$ Å^{-1}), unlike the scattering curve of the non-doped sample. This might be background scattering due to atomic scale ordering of the cobalt.

3.2.1. Reduced *versus* unreduced. Reduction of small metal clusters usually causes a shrinking of the cluster, which has been readily observed in several catalysts, such as Pt/C (Haubold *et al.*, 1996, 1999; Schlenter, 1996; Benedetti *et al.*, 1999). This is because metallic phases are characterized by dense packing. Fig. 4 displays the scattering curves of samples doped with 2% cobalt, in the non-reduced and the reduced state. Both scattering curves indicate a short plateau beginning at $q \leq 0.025$ Å^{-1}, and ending at 0.009 Å^{-1} for the reduced sample and at 0.015 Å^{-1} for the unreduced sample. We now look at the intensity in the plateau regime. The non-reduced sample has enhanced intensity for $q \leq 0.015$ Å^{-1}, *i.e.* the intensity exceeds the height of the plateau. The reduced sample shows this effect only for $q \leq 0.009$ Å^{-1}. This can be interpreted as follows: the reduced sample shows larger objects in this q range than the non-reduced sample. In real space, this converts to an increase in size from 210 to 350 Å. Upon reduction, smaller objects vanish to be replaced by larger ones. This behavior seems surprising because we expect a decrease of the metal cluster upon reduction, not an increase.

The intensity power law in the range $0.0027 \leq q \leq 0.014$ Å^{-1} is about 2.1 for the non-reduced sample. The reduced sample shows a stronger power law, indicating that the particles in this size range become more isometric upon reduction. If the particles in this range were elongated in one or two dimensions, such as rods or plates, then the power law would be less steep. The asymptotic exponent of decay for

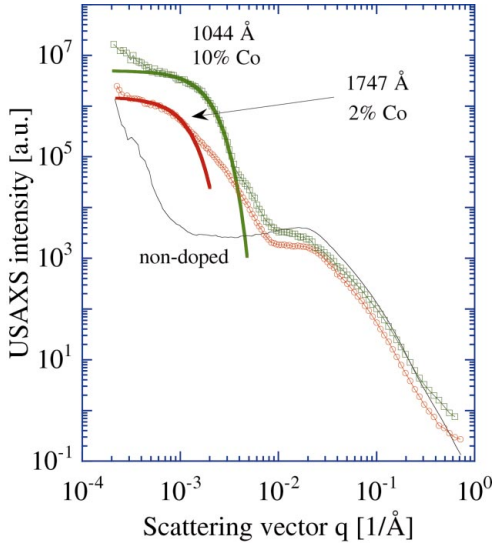

Figure 3
Scattering curves of non-doped (thin scattering curve) and 10%-doped (squares) and 2%-doped (circles) samples. Drawn lines in the scattering curves from doped samples denote least-squares fits of the Guinier function.

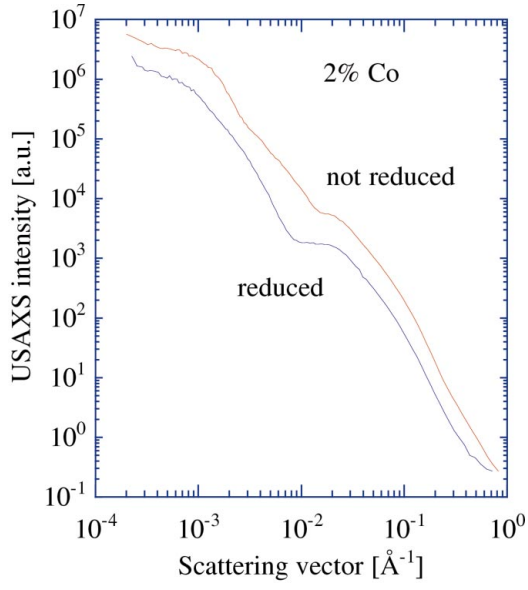

Figure 4
Comparison of the scattering curves of reduced and unreduced samples with 2% cobalt.

spherical shells and for large, thin planar objects (like sheets) is typically 2. The objects in this size range in the non-reduced aerogel could therefore be either sphere-like shells or largely extended, thin sheets. With the data available so far, it is not possible to determine the exact scenario that occurs during reduction.

Ostwald ripening, where smaller clusters coagulate to larger ones (the signature of the smaller objects would vanish, and the signature of a new larger structure would occur, as observed here), would be one possible hypothesis, but we believe that a re-ordering of elongated particles towards a more isometric shape during reduction is the more realistic scenario.

We have looked also at the large q tails of the scattering curves of the 10%-doped samples and found no significant size changes upon doping or upon reduction, as becomes clear in Fig. 5. However, it seems that the non-doped samples have the sharpest size distribution, while the most diffuse size distribution stems from the unreduced samples. Upon reduction, the scattering curves adopt again a somewhat sharper size distribution.

3.2.2. Skin effect during aerogel formation. The aerogel samples were supplied as cylinders with obvious rotational symmetry. However, with respect to the cylinder axis, the samples seemed to be inhomogeneous in terms of their color and outer appearance, such as if the samples had a 'skin'. It was thus possible to carry out a spatially resolved, or radius-resolved measurement by exposing either the sample center or the sample boundary to the X-ray beam. It is possible to perform a scattering experiment with a spatial resolution of about 1 mm, thus allowing cross-section experiments with the samples. It should be possible to detect Liesegang patterns with this technique (Samseth *et al.*, 1998). Fig. 6 displays the scattering curves of experiments where either the sample center (no skin) or the sample boundary (much skin) were measured. The scattering curves show significant differences in the low-q region. Intensity oscillations in the central part of either curves are a strong indication of a relatively sharp particle size distribution. The lines show the least-squares fits to a Guinier function. The radius of gyration is 845 Å for the center of the sample, while for the sample boundary an R_g of 1135 Å is found. In the Guinier analysis, we have neglected the intensity oscillations. More rigorous analysis was performed, however, and will be presented in the next section for all samples.

3.2.3. Quantitative analysis with unified fit and size distribution. The overall scattering of the samples shows that the aerogels are rich and manifold in structure. Overlap of Guinier scattering and power law scattering makes quantitative analysis difficult. Modelling the scattering curve at small scattering vectors with structure factors and size distribution functions yields more accurate results (Braun *et al.*, 1999). The unified fit (Beaucage, 1995) accounts for overlap in medium and large scattering vectors and also yields more accurate results. We will briefly write the formula for the unified fit, which is basically a sum of Guinier scattering and power law scattering:

$$I(q) = G\exp(-q^2R_g^2/3) + B\left\{[\mathrm{erf}\,(qR_g/6^{1/2})]^3/q\right\}^P, \quad (4)$$

with the error function erf and exponent of decay, P. The prefactors G and B contain quantities such as material densities, internal surface areas, particle numbers. The expressions in equation (4) are basic building blocks which can be combined to model several Guinier and power law ranges in a scattering curve (Fig. 7). The unified fit was applied locally to the structures $q \geq 0.01$ Å^{-1}. For the structures $q \leq 0.01$ Å^{-1}, spheres were assumed as scatterers, and Gaussian size distribution was applied. Mean diameters and full width at half-maximum values of the size distribution of the cobalt particles are given in the column 'largest level' in Table 1. Gaussian size distribution yields the visually best fits to the scattering data. However, within the context of a particle size

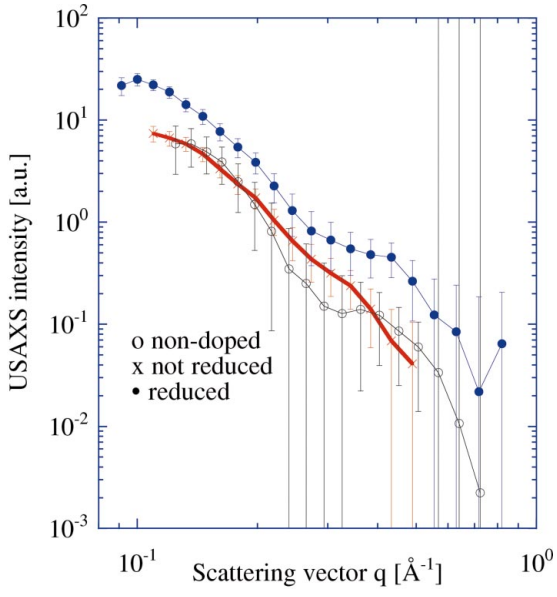

Figure 5
Comparison of the large q tails of the scattering curves of non-doped aerogel, and of reduced and unreduced samples with 10% cobalt.

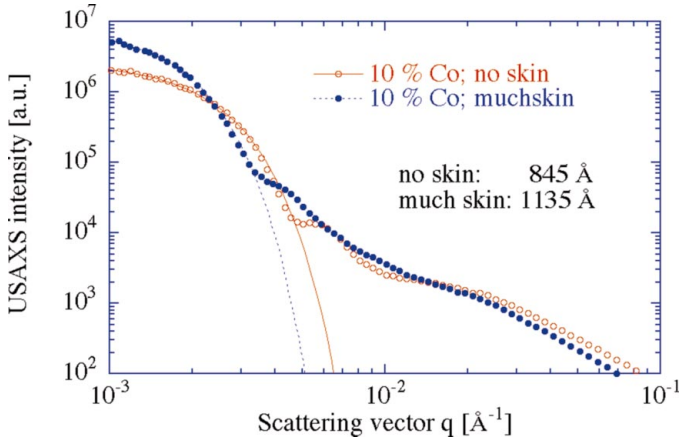

Figure 6
Scattering curves of 10% Co-doped samples from the center (no skin) and from the boundary (much skin).

Table 1
Radii of gyration of the first three size levels, as obtained from unified fit (Beaucage, 1995).

The largest size level was fitted to the structure factor of spheres, including a Gaussian size distribution function.

Sample	Finest level R_g (Å)	Level 2 R_g (Å)	Level 3 R_g (Å)	Largest level Mean diameter; FWHM (Å)
CO_2 dried, non-doped	4.7 ± 3.5	34.5 ± 1.6	71.5 ± 2.5	–
EtOH dried, non-doped	11.0 ± 2.8	46.6	55.0 ± 5	–
10% Co, no skin	10.6 ± 1.0	46.7 ± 0.3	64.5 ± 3.5	1880; 611
10% Co, skin	7.5 ± 30.3	21.9 ± 1.7	80.6 ± 1.4	2248; 1189
10% Co, not reduced	6.1 ± 1.1	17.1 ± 0.5	72.4 ± 1.0	1501; 1627
10% Co, reduced	6.4 ± 0.7	17.7 ± 0.5	68.1 ± 0.7	∼2100
10% Co, not reduced	7.2 ± 0.8	20.0 ± 1.6	68.1 ± 1.3	∼2127
2% Co, reduced	7.3 ± 1.3	18.0 ± 0.6	62.8 ± 0.7	∼3000
2% Co, not reduced	6.4 ± 0.6	17.6 ± 0.4	63.0 ± 1.2	∼2400
2% Co, 7695 eV, reduced	8.9	25.3	61.1	∼1000, 2000, 4400
2% Co, 7695 eV, not reduced	8.2 ± 0.8	18.1 ± 0.61	68.2 ± 1.1	∼2400
10% Co, 7710 eV, reduced	7.4 ± 0.6	29.1 ± 4.5	67.0 ± 3.9	∼2200
10% Co, 7710 eV, not reduced	8.3 ± 1.5	20.6 ± 2.0	68.2 ± 1.4	∼2210
2% Co, 7710 eV, reduced	4.5 ± 0.9	36.1 ± 1.7	66.4 ± 3.7	More populations
2% Co, 7710 eV, not reduced	4.8 ± 0.7	36.6 ± 1.7	73.6 ± 2.3	∼2253

distribution, a Gaussian distribution is physically not justified. Often a log-normal distribution is used for particle size distributions obtained from scattering experiments. The use of the log-normal distribution lies more in the computational convenience than in physical justification, because the product of lognorm with any power of its arguments is analytically integrable. Using a Lifshitz–Slyozov–Wagner (LSW) distribution (Lifshitz & Slyozov, 1961; Wagner, 1961) yields least-squares fits as good as a lognormal distribution does. The LSW distribution for spheres with radius R reads as follows:

$$P(R) = \frac{3^4 R^2 \exp[-1/(1-2R/3)]}{2^{5/3}(R-3)^{7/3}(3/2-R)^{11/3}}. \qquad (5)$$

Fig. 8 shows the scattering curve for the 10% Co-doped reduced aerogel, measured at the aerogel cylinder-axis position. The solid line represents the least-squares fit of an LSW distribution to the data. The fit basically reproduces all

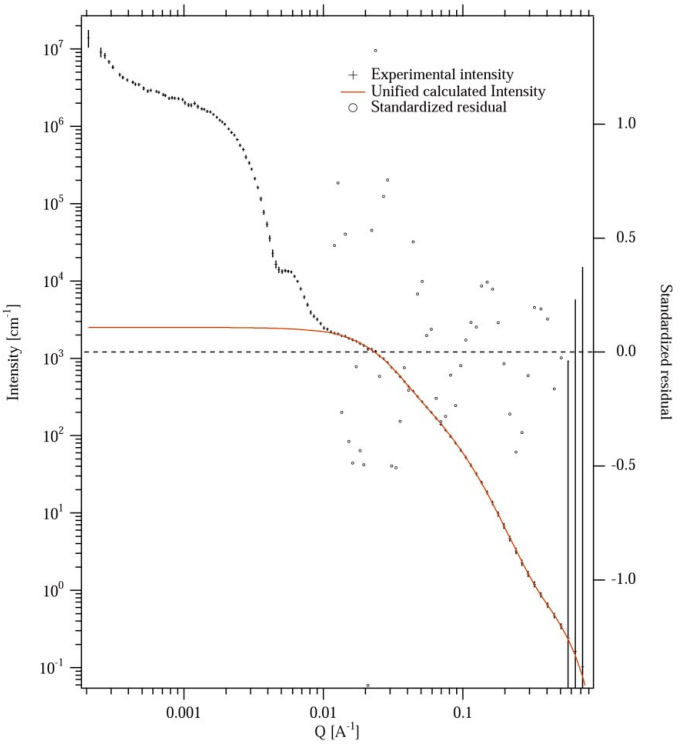

Figure 7
Scattering curve of the 10% Co-doped sample from the center, measured at the sample cylinder-axis position. The solid line is the unified fit with three Guinier ranges and three power laws

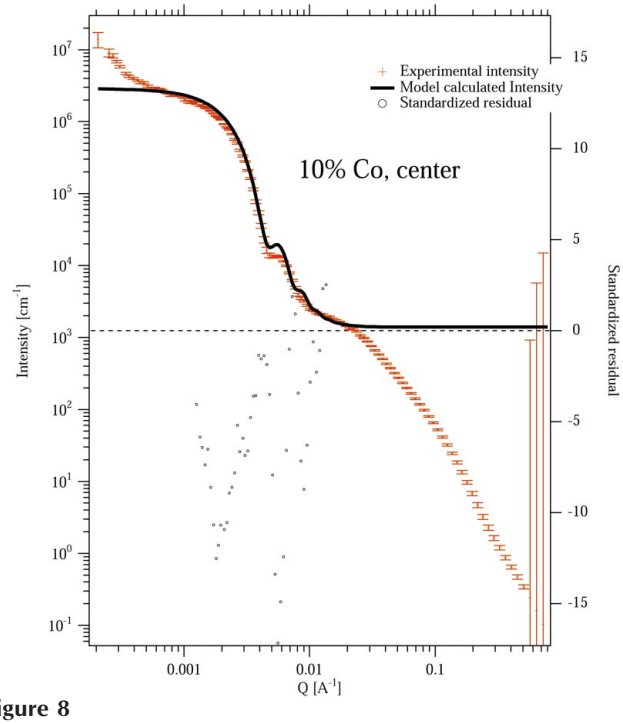

Figure 8
Scattering curve of the 10% Co-doped sample from the center, measured at the sample cylinder-axis position. The solid line is the fit with assumed spheres and size distribution characteristic of Ostwald ripening (Lifshitz–Slyozov–Wagner).

experimentally observed intensity minima that we can assign to the cobalt precipitates, with minor deviations in intensity height that can arise from mismatch with the medium-q range of the scattering curve. The LSW fit was well applicable to all 10%-doped samples. The corresponding fit for the 2% doping level was more problematic, including the Gaussian fit. This is particularly because the shape of the scattering curve seems to be dominated by a $q^{-2.1}$ power law, as already mentioned, with superimposed intensity oscillations (Fig. 4, the 'not reduced' sample). It was observed (Martino *et al.*, 1999) that calcination of sol–gel based nanocluster catalysts at 723 K causes metal cluster coagulation and coarsening by Ostwald ripening, rather than by diffusion, depending on the metal coverage. It is thus likely that a similar sintering process is observed in our studies, indicated by the good match of the LSW fit and the scattering data.

4. Summary

Silica aerogels were doped with cobalt, reduced, and studied with ultra-small-angle X-ray scattering. A scattering pattern rich in structure extends over nearly four orders of magnitude in q space, covering real space from 5 to 3000 Å, exposing micropores, mesopores and macropores for all aerogels. The Co-doped aerogels show precipitates with sizes of several thousand ångströms. USAXS allows us to distinguish reduced samples from unreduced samples and to monitor process-related inhomogeneities in the sample, such as skin effects. We believe that anomalous scattering would yield more precise information about particle size distributions.

This research received financial support from the US Department of Energy to the Consortium for Fossil Fuel Science, of which the University of Kentucky and University of Utah are both members. USAXS was performed at the UNICAT facility at the Advanced Photon Source (APS), which is supported by the University of Illinois at Urbana-Champaign, Materials Research Laboratory (US DOE, the State of Illinois-IBHE-HECA, and the NSF), the Oak Ridge National Laboratory (US DOE under contract with UT-Battelle LLC), the National Institute of Standards and Technology (US Department of Commerce) and UOP LLC. The APS is operated by the University of Chicago for US Department of Energy, Basic Energy Sciences, Office of Science, under contract No. W-31-109-ENG-38.

References

Bazin, D., Mottet, C., Tréglia, G. & Lynch, J. (2000). *Appl. Surf. Sci.* **164**, 140–146.
Beaucage, G. (1995). *J. Appl. Cryst.* **28**, 717–728.
Benedetti, A., Bertoldo, L., Canton, P., Goerigk, G., Pinna, F., Riello, P. & Polizzi, S. (1999). *Catal. Today*, **49**, 485–489.
Braun, A., Bärtsch, M., Schnyder, B., Kötz, R., Haas, O., Haubold, H.-G. & Goerigk, G. (1999). *J. Non-Cryst. Solids*, **260**, 1–14.
Casula, M. F., Corrias, A. & Navarra, G. (2003). *J. Sol-Gel Sci. Technol.* **26**, 453–456.
Emmerling, A. & Fricke, J. (1992). *J. Non-Cryst. Solids*, **145**, 113–120.
Glatter, O. & Kratky, O. (1982). *Small-Angle X-ray Scattering*. New York: Academic Press.
Guinier, A. (1939). *Ann. Phys.* **12**, 161–237.
Haubold, H.-G., Hiller, P., Jungbluth, H. & Vlad, T. (1999). *Jpn J. Appl. Phys.* **38**(1), 36–39 (Suppl. 38-1, Proc. Int. Conf. SRMS-2).
Haubold, H.-G., Wang, X. H., Jungbluth, H., Goerigk, G. & Schilling, W. (1996). *J. Mol. Struct.* **383**, 283–289.
IUPAC (1985). *Pure Appl. Chem.* **57**, 603–620.
Jemian, P. R. & Long, G. G. (1990). *J. Appl. Cryst.* **23**, 430–432.
Lifshitz, I. M. & Slyozov, V. V. (1961). *J. Phys. Chem. Solids*, **19**, 35–50.
Lorenz, C., Emmerling, A., Fricke, J., Schmid, T., Hilgendorff, M., Spanhel, L. & Müller, G. (1998). *J. Non-Cryst. Solids*, **238**, 1–5.
Marliére, C., Woignier, T., Dieudonné, P., Primera, J., Lamy, M. & Phallippou, J. (2001). *J. Non-Cryst. Solids*, **285**, 175–180.
Martino, A., Sault, A. G., Kawola, J.S., Boespflug, E. & Phillips, M. L. F. (1999). *J. Catal.* **187**, 30–38.
Porod, G. (1951). *Kolloid-Z.* **124**, 83–114.
Porod, G. (1952*a*). *Kolloid-Z.* **125**, 51–57.
Porod, G. (1952*b*). *Kolloid-Z.* **125**, 109–122.
Lord Rayleigh (1911). *Proc. R. Soc. London Ser. A*, **84**, 25–46.
Russo, R. E. & Hunt, A. J. (1986). *J. Non-Cryst. Solids*, **86**, 219–230.
Samseth, J., Kirkdelen, M. B., Maaø, F. A., Hansen, A. & Einarsrud, M.-A. (1998). *J. Non-Cryst. Solids* **225**, 298–302.
Schaefer, D. W. & Keefer, K. D. (1986). *Phys. Rev. Lett.* **56**, 2199–2202.
Schlenter, M. (1996). *Röntgenkleinwinkelstreuung und XANES-Messungen an kohlen stoffgeträgerten Platinkatalysatoren*, Diploma thesis, Rheinisch-Westfälische Technische Hochschule Aachen, Germany (unpublished).
Vacher, R., Woignier, T., Pelous, J. & Courtens, E. (1988). *Phys. Rev. B*, **37**, 650–6503.
Wagner, C. Z. (1961). *Elektrochem. (Ber. Bunsenges. Phys. Chem.)* **65**, 581–591.